Clustering instabilities, Arching and Anomalous Interaction Probabilities as Examples for Cooperative Phenomena in Dry Granular Media

S. Luding
Institute for Computer Applications 1,
Pfaffenwaldring 27, D-70569 Stuttgart, GERMANY

April 3, 1998

Abstract

In a freely cooling granular material fluctuations in density and temperature cause position dependent energy loss. Due to strong local dissipation, pressure and energy drop rapidly and material moves from 'hot' to 'cold' regions, leading to even stronger dissipation and thus causing the density instability. The assumption of 'molecular chaos' is valid only in the homogeneous cooling regime. As soon as the density instability occurs, the impact parameter is not longer uniformly distributed. The pair-correlation and the structure functions show that the molecular chaos assumption — together with reasonable excluded volume modeling — is important for short distances and irrelevant on large length scales.

In this study, the probability distribution of the collision frequency is examined for pipe flow and for freely cooling granular materials as well. Uncorrelated events lead to a Poisson distribution for the collision frequencies. In contrast, the fingerprint of the cooperative phenomena discussed here is a power-law decay of the probability for many collisions per unit time.

Keywords:
discrete element method, event driven simulations, clustering instability, arching, shock waves, Poisson distribution, cooperative phenomena.

1 Introduction

Many rather astonishing phenomena are known to occur when granular materials like sand or powders move [1–4]. Of interest are, e.g. density waves emitted from outlets [5], crack formation during vibration or during the flow through a pipe [6–9], and pattern formation due to dissipation [10–14]. All these effects are connected to the ability of granular materials to form a hybrid state between a fluid and a solid: energy input can lead to a reduction of density so that the material becomes 'fluid' and, on the other hand, in the absence of energy input, granular materials 'solidify' due to dissipation. Thus, a packing of sand behaves like a solid when pushed, but offers no resistance to a pulling force.

In order to formalize and quantify the complicated rheology of granular media various attempts have been made. Continuum equations of motion and kinetic theories [4, 15–21] are the first successful steps towards a quantitative description of granular materials — at least for limited parameter range. This restriction exists because it is very difficult to incorporate into these theories all the details of static friction or other relevant microscopic mechanisms. Also the generalization to high densities is an ardous task, see for example Refs. [22, 23] and references therein. Most of the classical, but also the more advanced theories are based on the assumption of molecular chaos — the assumption that the velocities and positions of all colliding pairs of particles in a gas are uncorrelated. In a dilute gas, the errors introduced by this assumption are negligible. In dense granular flows, however, correlations between colliding particles may be important, leading to qualitative changes of behavior.

Section 2 is dedicated to a brief introduction of the different discrete modeling approaches. In particular, we will present the 'hard-particle' Event Driven (ED) [24, 25] and the 'soft-particle' Molecular Dynamics (MD) [24, 26, 27] methods, both for inelastic spherical particles with frictional forces. We extend the traditional ED method by introducing a cut-off time for dissipation [3, 12]. Any particles that encounters a second collision before this time passed by is assumed to be elastic — the extended method is named TCED. Furthermore, the Direct Simulation Monte Carlo (DSMC) approach is discussed and applied to freely cooling granular media. The validity of the molecular chaos assumption in granular flows was examined by comparing event driven (ED) 'hard sphere' simulations to those performed with the Direct Simulation Monte Carlo (DSMC) method [14]. The ED method is capable of reproducing velocity correlations — even in the limit of rather large densities — whereas DSMC assumes molecular chaos by construction. In Section 3 the structure factor and the pair-correlation function are examined and reasons for the breakdown of molecular chaos are discussed. The clustering instability is described in Section 4 with respect to the restitution coefficient and a cut-off time for dissipation. The probability distribution function for the collision frequency is measured in the homogeneous and the non-homogeneous clustering case and differences in the functional behavior are evidenced [3]. The same behavior is also found in pipe flow [9] where shock waves and arching are the observed cooperative phenomena. The probability distribution functions are measured and discussed in Section 5 and interestingly have the same functional behavior as in the case of the clustering instability. Finally, the results are summarized in Section 6.

2 Models for particle-particle interactions

The basic constitutents of granular materials are mesoscopic grains, made of, for example, 10^{20} molecules. When these objects interact (collide) the attractive potentials of the individual atoms can often be neglected. Three models for the particle-particle interactions are discussed in the following. They account for the excluded volume of the particles via a repulsive potential, either 'hard' or 'soft', or assume point particles and introduce appropriate corrections.

It is important that the surface of the grains is rough on a microscopic scale so that solid friction occurs. In general, one has to distinguish between sliding, sticking, and rolling friction, but we will only discuss simplified models here. An entire discipline called tribology has evolved to study solid friction in depth [1, 28]. Friction and other sources of dissipation, like viscous damping or plastic deformations, have the crucial consequence that the system *does not conserve energy.* Since dissipation may occur due to various reasons, we discuss in the following only simple dissipation laws, assuming that the detailed knowledge of the interaction potential is of minor importance. In fact, complicated laws often increase the number of parameters without giving qualitatively different results [29].

The difference between the two most frequently used discrete element methods is the repulsive interaction potential. For the molecular dynamics (MD) method, soft particles with a power-law interaction potential are assumed, whereas for the event driven (ED) method perfectly rigid particles are used. The consequence is that the duration of the contact of two particles, t_c, is finite for MD, but vanishes for ED. In the DSMC method, one assumes point particles without repulsive potential but with an effective scattering cross section. In addition one applies corrections from the kinetic theory, in order to account for the effective free volume, the reduced mean free path, the increased collision frequency and the modified momentum transport.

2.1 The event driven, rigid particle method

Here, we apply the simplified collision model introduced by Walton and Braun [30] and recently experimentally established by Foerster et al. [31] and Labous and Rosato [32]. For given velocities before contact, three coefficients are needed to evaluate the velocities after collision. At first, the coefficient of normal restitution, r, defines the incomplete restitution of the normal component of the relative velocity. The second, the coefficient of friction, μ, relates the tangential momentum change to the normal one, i.e. Coulomb's law. The third, the coefficient of maximum tangential restitution, β_0, delimits the restitution of tangential velocity of the contact point to ensure energy conservation. Note that this model implies that two grains at contact either slide, following Coulomb's law, or stick together [30, 31, 33, 34]. In the following, we apply the basic conservation laws and determine the equations for the velocities after collision.

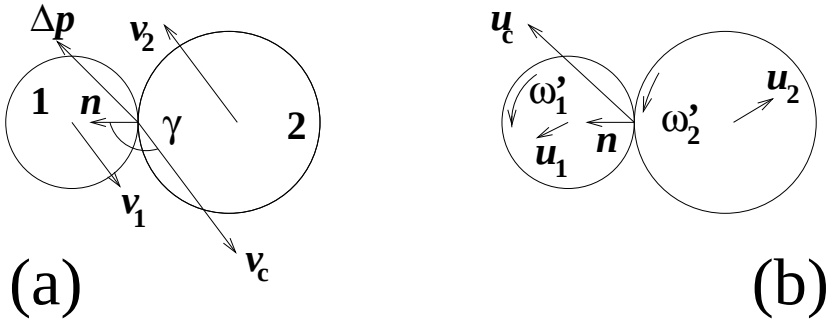

Figure 1: Typical velocities of two particles immediately before (a) and after (b) collision.

Consider two particles with diameter d_1 and d_2 and masses m_1 and m_2. The normal unit vector for their contact is $\vec{n} = (\vec{r}_1 - \vec{r}_2) \,/\, |\vec{r}_1 - \vec{r}_2|$, where $\vec{r}_i$ is the vector that gives the position of the center of particle i ($i = 1, 2$). For the interaction of particle $i = 1$ with a fixed wall, we set $m_2 = \infty$, and $\vec{n}$ is in this case the unit vector perpendicular to the wall surface pointing from the contact point with the wall to the center of the particle. The relative velocity of the contact points is

$$\vec{v}_c = \vec{v}_1 - \vec{v}_2 - \left(\frac{d_1}{2}\vec{\omega}_1 + \frac{d_2}{2}\vec{\omega}_2\right) \times \vec{n} \ , \tag{1}$$

with $\vec{v}_i$ and $\vec{\omega}_i$ being the linear and angular velocities of particle i just before collision. From the momentum conservation laws for linear and angular momentum follows

$$\vec{v}_1' = \vec{v}_1 + \Delta\vec{P}/m_1 \tag{2}$$

$$\vec{\omega}_1' = \vec{\omega}_1 - \frac{d_1}{(2I_1)}\vec{n} \times \Delta\vec{P} \ , \tag{3}$$

$$\vec{v}_2' = \vec{v}_2 - \Delta\vec{P}/m_2 \ \text{, and} \tag{4}$$

$$\vec{\omega}_2' = \vec{\omega}_2 - \frac{d_2}{(2I_2)}\vec{n} \times \Delta\vec{P} \ , \tag{5}$$

where $\vec{v}_i'$ and $\vec{\omega}_i'$ are the unknown velocities of particle i after collision. I_i is the moment of inertia about the center of particle i and $\Delta\vec{P}$ is the change of linear momentum of particle 1 and is a function of r, μ, and β_0:

$$\Delta\vec{P} = -m_{12}(1+r)\vec{v}_c^{(n)} - \frac{2}{7}m_{12}(1+\beta)\vec{v}_c^{(t)}, \tag{6}$$

with the reduced mass $m_{12} = m_1 m_2/(m_1 + m_2)$. (n) and (t) indicate the normal and the tangential components of $\vec{v}_c$, respectively, and the factor $2/7$ in the tangential part of Eq. (6) stems from the fact that solid spheres are used [34]. r is the coefficient of normal restitution and $\beta = \min[\beta_0, \beta_1]$ is the coefficient of tangential restitution. The latter is simplified so that either sticking or sliding are exclusively allowed. A sticking contact has a constant maximum tangential restitution $\beta = \beta_0$, with $-1 \leq \beta_0 \leq 1$ due to the elasticity of the material. Typical values for, e.g. acetate or glass, are $\beta_0 \approx 0.5$ [31]. Sliding, Coulomb-type interactions have $\beta = \beta_1$, i.e. $\Delta P^{(t)}$ is limited by $\mu_w \Delta P^{(n)}$. Using the basic conservation laws one can find $\beta_1 = -1 - \mu(1+r)\cot(\gamma)(1 + 1/q_i)$, with the collision angle γ, and the factor $q_i = 4I_i/(m_i d_i^2)$ that accounts for the mass distribution inside the particles [31, 33, 34]. As illustration, a schematic picture of two colliding particles is given in Fig. 1. The angular velocities are $\omega_1 = \omega_2 = 0$ immediately before collision (a) and non-zero after collision (b). For a more detailed discussion of the above equations see Ref. [33, 34].

For the simulation of rigid particles, we use an event driven method such that the particles undergo an undisturbed motion until an event occurs. An event is either the collision of two particles or the collision of one particle with a wall. From the velocities just before contact, the particle velocities after a contact are computed following Eqs. (2)-(5). Lubachevsky [25] introduced an efficient scalar ED algorithm which updates only those particles involved in the previous collision. Like in Refs. [29,33] we implement the algorithm of Ref. [25] with some changes and extensions. Despite gravitational acceleration, all times of contact of particles with each other or with the lateral walls can be calculated analytically. The coefficient of normal restitution depends on the partner of the colliding particle, i.e. r or r_w is used to indicate particle-particle, or particle-wall collisions, respectively.

2.2 The connection between hard- and soft-sphere models

In the ED method, the time during which two particles are in contact is implicitly zero. The consequence is that exclusively pair contacts occur and the instantaneous momentum change $\Delta\vec{P}$ in Eqs. (2)-(5) suffices to describe the collision completely. ED algorithms with constant r run into difficulties when the time between events, $t_{\rm ev}$, becomes too small — typically in systems with strong dissipation — and the so-called 'inelastic collapse' occurs [35–38]. To handle this problem, several attempts have been proposed recently [3, 12, 38–44], and one of them [3, 12] switches off dissipation when the collision frequency becomes too large.

In MD simulations of dynamical systems, on the other hand, $t_c > 0$ and only a limited amount of energy can be dissipated per contact. A finite contact duration thus implies a finite energy dissipation rate. In a dense system of soft particles, energy dissipation becomes ineffective, i.e. the 'detachment effect' occurs [45, 46]. This effect is not obtained with hard particles and a constant coefficient of restitution r, however, the effect can be observed when using

$$r_n^{(i)} = \begin{cases} r & \text{for} \quad t_n^{(i)} > t_c \\ 1 & \text{for} \quad t_n^{(i)} \le t_c \ , \end{cases} \tag{7}$$

as the restitution coefficient for the collision n of particle i. In Eq. (7) $t_n^{(i)}$ is the time since the last collision and t_c is the threshold for elastic contacts that can be identified (up to a constant factor of order unity) with the contact duration in the soft particle model. Thus, an additional material parameter is defined for the hard sphere model, that leads to qualitative agreement between ED and MD simulations and in addition avoids the inelastic collapse. Note that t_c has different physical meaning in either hard or soft sphere model. The traditional ED method has $t_c = 0$. The extended model that uses Eq. (7) with $t_c > 0$ is in the following referred to as the TCED method.

The integral of all forces $\vec{f}(t)$, acting on a particle at time $t \in [t_0,\ t_c]$, is needed to calculate the momentum change of this particle in the framework of the soft particle model:

$$\Delta\vec{P} = \int_{t_0}^{t_c} \vec{f}(t)\mathrm{d}t \ . \tag{8}$$

In general, the contact begins at time t_0 and ends at time t_c. For a constant force $\vec{f}$ or an infinitesimally small time interval $t_c - t_0$, the momentum change $\Delta\vec{P}$ in Eqs. (2)-(5) can be replaced by the term $f(t)\mathrm{d}t$ to arrive at a differential formulation for the change of velocities $\vec{v}' - \vec{v}$ and $\vec{\omega}' - \vec{\omega}$. The primed and unprimed quantities are the values at time t_c and t_0, respectively.

The stress tensor, defined for a test volume V_c, can be written as

$$\sigma_{\alpha\beta} = \frac{1}{V_c}\left[\sum_j r_\alpha f_\beta - \sum_i m_i v_\alpha v_\beta\right] . \tag{9}$$

The indices α and β are the Cartesian coordinates, r_α are the components of the vector from the center of mass of a particle to the point j, where a force with components f_β acts. Particle i has the mass m_i and a velocity with the components v_α. The first sum runs over all contact points j, and the second sum runs over all particles i, both within V_c. In the static limit, the second term vanishes, since all velocities vanish. On the other hand, for a hard-sphere gas, the left term has to be treated differently, since no forces are defined. The dynamic equivalent to f_β is the change of momentum per unit time $\Delta P_\beta/\Delta t$. For a hard-sphere gas the stress due to collisions may be evaluated as the

average over all collisions in the time interval Δt. The first sum runs over all collisions taking place in the time between $t - \Delta t$ and t. In general, the volume V_c and the time-interval Δt have to be chosen large enough to allow averages over enough particles and enough collisions.

2.3 The time driven, soft particle technique

Even without using the soft particle method in this study, it is convenient to discuss briefly the standard interaction forces and their connection to the hard sphere collision operator that involves the total momentum change $\Delta\vec{P}$. Replacing $\Delta\vec{P}$ in Eqs. (2)-(5) by $\vec{f}(t)t_{\rm MD}$, with the molecular dynamics time step $t_{\rm MD}$, allows the integration of the corresponding equations of motion with standard numerical methods [24, 27].

Since the modeling of realistic deformations of the particles would be much too complicated, let us assume that the overlap of two particles is the quantity important for the interaction potential. The interaction is short range, i.e. the particles interact only when they are in contact so that their penetration depth $\delta = \frac{1}{2}(d_1 + d_2) - (\vec{r}_1 - \vec{r}_2) \cdot \vec{n}$ is positive.

The first force, acting from particle 2 on particle 1 — accounting for the excluded volume which each particle occupies — is an elastic repulsive force

$$\vec{f}_{\rm el} = k_n \delta_0 (\delta/\delta_0)^\nu \vec{n} \ , \tag{10}$$

where k_n is the elastic modulus and δ_0 is a normalization constant dependent on the nonlinearity ν and the dimension. In the simplest case of a linear spring that follows Hooke's law, $\nu = 1$, in the case of elastic spheres in three dimensions, $\nu = 3/2$ i.e. a Hertz contact [47], and for conical contacts, $\nu = 2$ can be used.

The second force — accounting for dissipation in the normal direction — is a viscous damping force

$$\vec{f}_{\rm diss} = \gamma_n \dot{\delta} (\delta/\delta_0)^\phi \vec{n} \ , \tag{11}$$

where γ_n is a phenomenological viscous dissipation coefficient and $\dot{\delta} = -\vec{v}_{12} \cdot \vec{n} = -(\vec{v}_1 - \vec{v}_2) \cdot \vec{n}$ is the relative velocity in the normal direction.

The simple linear spring-dashpot model (with $\nu = 1$ and $\phi = 0$) can be solved analytically and leads to a contact duration $t_c = \pi/\omega$ and a restitution coefficient $r = \exp(-\pi\eta/\omega)$, with $\omega = \sqrt{\omega_0^2 - \eta^2}$, $\omega_0^2 = k_n/m_{12}$, $\eta = \gamma_n/(2m_{12})$, and $m_{12} = m_1 m_2/(m_1 + m_2)$ [34]. A nonlinear repulsive potential can at least be solved in the limit $\gamma_n \to 0$ and the dependency of r on the velocity of impact can be estimated with reasonable accuracy [45, 48, 49].

The third force — accounting for friction — acts in the tangential direction and can be chosen in the simplest case as

$$\vec{f}_{\rm shear} = -\gamma_t \dot{\xi} \vec{t} \, , \tag{12}$$

where γ_t is the viscous damping coefficient in tangential direction and $\dot{\xi} = \vec{v}_{12} \cdot \vec{t}$ is the tangential component of the relative velocity, with $\vec{t} = \vec{v}_{12}/|\vec{v}_{12}|$. Eq. (12) is a rather simplistic description of shear friction. For many applications (arching, heap formation) it is, however, important to include more realistic static friction [1, 50] what can be realized by a virtual tangential spring [26, 51]: when two particles start to touch each other, one puts a virtual spring between the contact points of the two particles, and $\vec{\xi}(t_1) = \int_{t_0}^{t_1} [\vec{v}_{12}(t) \cdot \hat{t}(t)] {\rm d}t \ \hat{t}(t_1)$ is the *total tangential displacement* of this spring during the contact. The restoring frictional force is thus $-k_t\vec{\xi}$. According to Coulomb's criterion, the maximum value of the restoring force is proportional to the normal force $|f_n^c|$ at this contact, with the friction coefficient μ. Cast into a formula this gives a friction force

$$\vec{f}_{\rm fric} = -\frac{\vec{\xi}}{|\vec{\xi}|} \min(k_t|\vec{\xi}|, \mu f_n^c) \ . \tag{13}$$

We note that the tangential spring has to be kept at a maximum length $\xi_{\rm max} = \mu f_n^c/k_t$ in order to lead to reasonable agreement with contact dynamics simulations or theoretical calculations [52]. Only when particles are no longer in contact with each other is the spring removed. The main source of static friction in real systems is the geometrical roughness of the surfaces [53–56], and the same

effects of particle stopping can be obtained also without Eq. (13) by using particles of complicated shapes, like crosses or polygons [57–60]. In fact, when particles deviate from the spherical shape, rotations are suppressed in dense packings under strong load. However, in some cases it is sufficient to use a combination of Eqs. (12) and (13):

$$\vec{f}_{\rm dyn} = -\min(\gamma_t \dot{\xi}, \mu f_n^c)\vec{t}\,, \tag{14}$$

a rather bold alternative to the more realistic static friction law in Eq. (13), but sufficient for many, especially dynamic situations [52]. For a comparison of ED and MD simulation results, see Refs. [29, 45, 52, 61].

2.4 DSMC simulation method

Direct simulation Monte Carlo (DSMC) was first proposed for the simulation of rarefied gas flows [62] and is also used for liquid-solid flow simulations, see Ref. [63] and references therein. One of the algorithm's advantages is its suitability for parallelization, what makes it a convenient tool for the modeling of granular media [34, 64].

In DSMC the evolution of the system is integrated in time steps τ, at each of which every particle is first moved without feeling other particles. The particles are then sorted into square cells with sides L_c and volume $V_c = L_c^2$. L_c is set as one half of the mean free path, but never smaller than two bead diameters. The time step τ is always chosen small enough to assure that even the fastest particle needs several time steps to cross a cell. Between particles in the same cell stochastic collisions take place; the rules for these collisions are taken from kinetic theory. First we choose the number of collision pairs in each cell,

$$M_c = \frac{N^c(N^c-1)\sigma v_{max}\tau}{2V_c}\,, \tag{15}$$

where N^c is the number of particles in the cell, v_{max} is an upper limit for the relative velocity between the particles, and $\sigma = 2d$ is the scattering cross section of discs in 2D. To get v_{max} we sample the velocity distribution from time to time and set v_{max} to be twice the maximum particle velocity found. In order to account for the actual relative velocities we apply an acceptance-rejection method: for a pair of particles i and j the collision is performed if

$$\frac{|\vec{v}_i - \vec{v}_j|}{v_{max}} < Z\,, \tag{16}$$

where Z is uniformly distributed in the interval $[0.0, 1.0[$. This method leads to a collision probability proportional to the relative velocity of the particles.

Since the collision takes place regardless of the position in the cell, we have to choose an impact parameter b in order to calculate the post-collision velocities. The impact parameter is defined as

$$b = \left|(\vec{r}_i - \vec{r}_j) \times \frac{(\vec{v}_i - \vec{v}_j)}{|\vec{v}_i - \vec{v}_j|}\right| = d\sin\gamma\,, \tag{17}$$

where γ is the angle between $(\vec{v}_i - \vec{v}_j)$ and $(\vec{r}_i - \vec{r}_j)$. For central collisions $b = 0$, and $b = d$ for grazing collisions. Assuming molecular chaos, b is drawn from a uniform distribution in the interval $[-d, d]$. The rest of the collision scheme is identical to the event driven procedure, so that the normal component of the post-collision velocity is $\vec{v'}^{(n)} = -r\vec{v}^{(n)}$, whereas the tangential component remains unchanged, i.e. $\beta_0 = -1$.

To get better results at higher densities the DSMC method was modified in two respects. First, the number of collisions M_c in equation (15) is increased by replacing the volume V_c of a cell with the effective free volume $V_c - V_0$, where V_0 is the volume the particles in that cell would need in a random close packing with packing fraction 0.82 in 2D [65]. Second, we added an offset of d to the particle distance along the direction of the momentum transfer after the collision [66].

3 Comparison of ED and DSMC simulations

In this section two simulations are presented, starting with the same initial condition, and using the same parameters, but being carried out with the ED and the DSMC methods. In ED the probability

distribution of the impact parameter may deviate from the case expected for molecular chaos, whereas DSMC always uses a constant probability for b in 2D. The simulations involve $N = 99856 = 316^2$ dissipative particles with restitution coefficient $r = 0.8$ in a periodic quadratic system with volume fraction $\varrho = 0.25$. The system size is $l = Ld$ with dimensionless size L and particle diameter d. In order to reach an equilibrated initial condition, the system is first allowed to evolve with $r = 1$ for about 10 collisions per particle, so that a Maxwellian velocity distribution and a rather homogeneous density distribution exists. Then, at $t = 0\,\mathrm{s}$, dissipation is set to $r = 0.8$ and the quantities of interest are calculated as functions of time.

3.1 Freely cooling granular materials

In the homogeneous cooling state [10, 17, 21, 67, 68] we expect that the energy $K(t)$ of the system decays with time and follows the functional form

$$\frac{K(t)}{K(0)} = \left(\frac{1}{1 + t/t_0}\right)^2 , \tag{18}$$

with the theoretically expected time scale

$$t_0 = \frac{\sqrt{\pi} d s_*(\varrho)}{2(1 - r^2)\varrho \bar{v}} \tag{19}$$

as a function of the initial mean velocity $\bar{v} = \sqrt{2K(0)/Nm}$, the particle diameter d, the restitution coefficient r, and the volume fraction ϱ with $s_*(\varrho) = (1 - \varrho)^2/(1 - 7\varrho/16)$ [17, 68–70]. Inserting the corresponding parameters $1 - r^2 = 0.36$, $s_*(\varrho) \approx 0.63158$, $d = 0.001\,\mathrm{m}$, and $\bar{v} = 0.2047\,\mathrm{m/s}$, we have $t_0^{-1} = 23.24\,\mathrm{s}^{-1}$.

In Fig. 2 we present the normalized kinetic energy $K(t)/K(0)$ as a function of the normalized time t/t_0. At the beginning of the simulation we observe a perfect agreement between the theory for

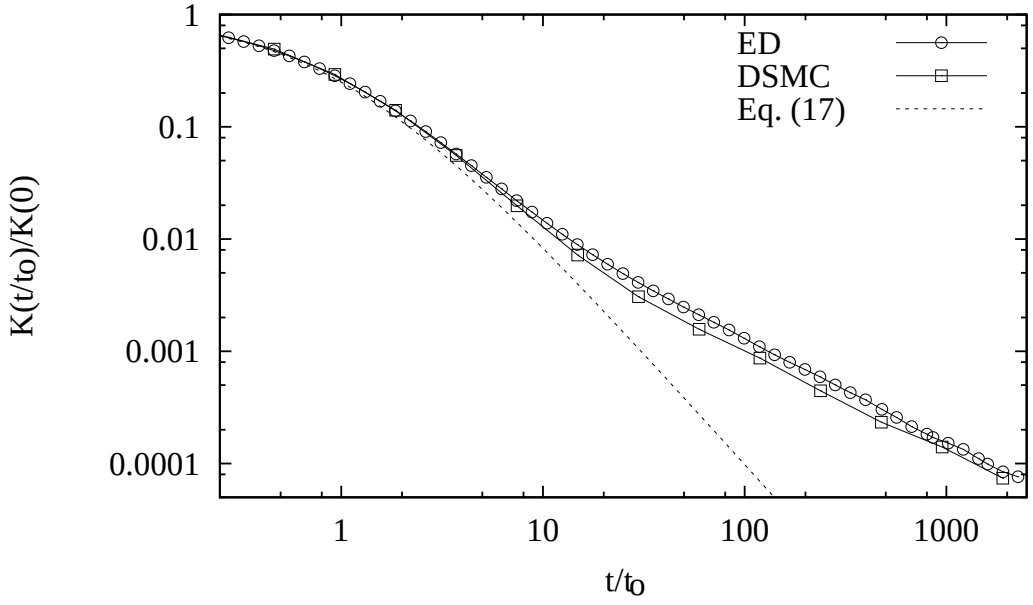

Figure 2: Normalized kinetic energy vs. normalized time from an ED and a DSMC simulation in 2D with identical initial conditions and $N = 99856$, $\varrho = 0.25$, $r = 0.8$. The dashed line represents Eq. (18).

homogeneous cooling and both simulations. At $t/t_0 \approx 2$ substantial deviations from the homogeneous cooling behavior become evident, and only at $t/t_0 \approx 10$ a difference between ED and DSMC can be observed. After that time, the kinetic energy obtained from the DSMC simulation is systematically

smaller than $K(t)$ from the ED simulation. We relate this to the fact that the molecular chaos assumption of a constant probability distribution of the impact parameter b is no longer valid. Since dissipation acts only at the normal component of the relative velocity, DSMC dissipates more energy than ED as soon as the number of central collisions is overestimated [14]. To verify this assumption we take a closer look at the impact parameter and its probability distribution in the next subsection.

3.2 The impact parameter

One basic assumption connected to molecular chaos is a uniform probability distribution of the impact parameter. We define $P(b/d)$ to be the probability distribution of b and normalize it such that $\int_0^1 \mathrm{d}x P(x) = 1$. We find from ED simulations with elastic particles the normalized probability distributions $P(b/d) = 1$ in 2D and $P(b/d) = 2b/d$ in 3D, as expected for the case of molecular chaos.

The ED simulation of Fig. 2 leads to $P(b/d) = 1$ for short times only. For larger times we observe an increasing (decreasing) probability of grazing (central) collisions. In Fig. 3, data of the probability distribution are presented at different times during the simulation of Fig. 2. As it is obvious from the data, more and more grazing collisions occur with increasing simulation time. Evidently, the assumption of a constant probability distribution of the impact parameter is violated.

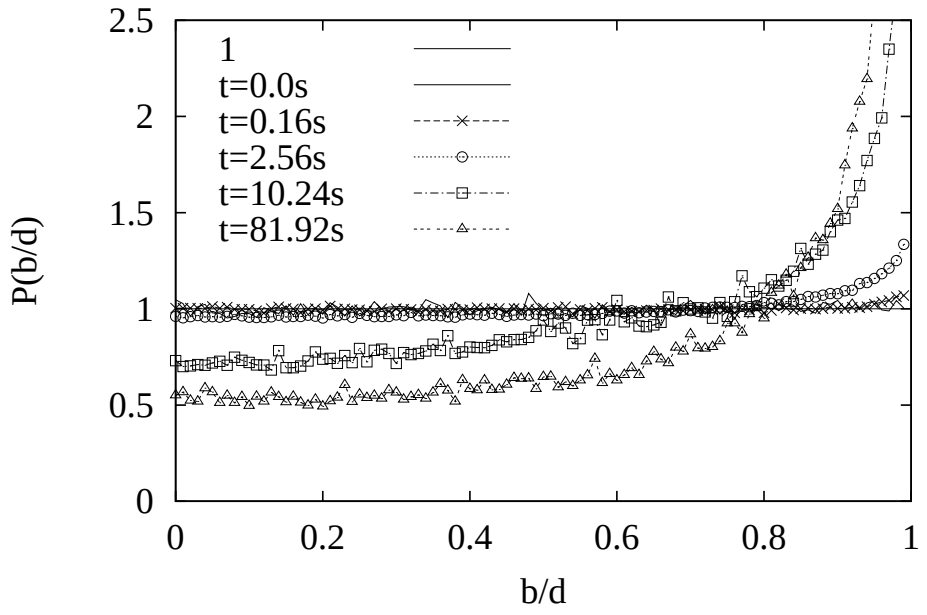

Figure 3: Normalized probability distribution of the contact parameter from an ED simulation in 2D with $N = 99856$, $\varrho = 0.25$, and $r = 0.8$ at different times, as given in the insert.

One can imagine at least two reasons for the deviation of $P(b/d)$ from the constant value. The first is that $P(b/d)$ might be a function of the density, and that due to density fluctuations, the form of $P(b/d)$ changes. Thus we calculate $P(b/d)$ in smaller systems with $N = 240$, $r = 1$, and different volume fractions, ranging from very dilute to extremely dense systems. $P(b/d)$ is not sensitive to the density, as long as the collisions are elastic [14]. Another reason for $P(b/d)$ to deviate from unity might be dissipation. In Fig. 4 the restitution coefficient is varied for fixed $\varrho = 0.7495$. For weak dissipation, i.e. $r \geq 0.9$, the distribution is homogeneous. For stronger dissipation $r = 0.80$ we find an increasing probability of grazing contacts.

The assumption $P(b/d) = 1$ is true in elastic systems for arbitrary density. For inelastic systems, $P(b/d)$ is constant for sufficiently weak dissipation but depends on b/d for strong dissipation. The breakdown of molecular chaos is *not due to high density*, and also *dissipation is not the only reason* for it, since the dissipation must be strong enough to cause the inhomogeneous distribution.

The remaining question is: why do we observe this increasing probability of grazing contacts?

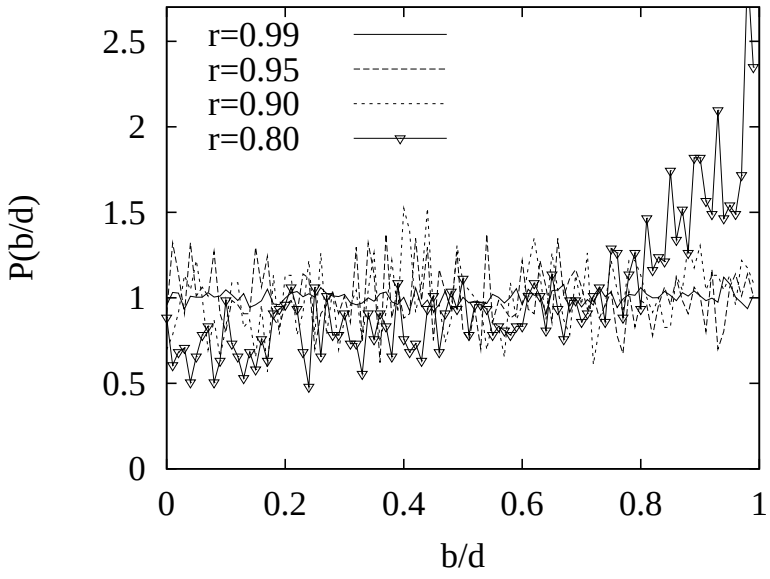

Figure 4: Normalized probability distribution $P(b/d)$ from ED simulations in 2D with $N = 240$, $\varrho = 0.7495$ and different r.

Looking in more detail at the simulations in Fig. 4, we observe that the inhomogeneous distribution for $r = 0.8$ is connected to shear motion of the particles, whereas no visible shear motion occurs for $r \geq 0.9$. The shear motion in the left panel of Fig. 5 can be understood as the geometrical reason for the higher probability for grazing contacts, i.e. layers of particles shear against each other and therefore touch preferentially with large impact parameter b. The two eddies (top left and bottom right) in the left panel are rotating in the same sense and lead to small stresses in the interior. Outside, where the velocities are less correlated one observes larger stresses and the stress tensor typically has strongly different eigenvalues. The more disordered situations in the middle and right panel, in contrast, are connected to rather random stresses.

3.3 The structure factor

One difference between ED and DSMC simulations is the handling of excluded volume by the two methods. While the ED method models hard spheres with a well defined excluded volume, the DSMC method models point particles and excluded volume is introduced by the approximations described in subsection 2.4. As expected, we obtain dramatic differences in the particle-particle correlation function $g(r/d)$ in Fig. 6, where r/d is the particle separation in units of particle diameters d. Since ED (solid lines) models hard spheres, $g(r/d) = 0$ when $0 \leq r/d < 1$. For short times one observes g as for an elastic hard sphere gas and at larger times $g(r/d)$ shows a rich structure with peaks at 1, 2, 3, ... and multiples of $\sqrt{3}/2$, indicating a rather close packing of monodisperse spheres. In contrast, the DSMC simulations (dashed lines) show no short range correlations between particle positions throughout the whole simulation.

The next question is, whether this difference has consequences at longer length scales. The formation and growth of large clusters [10, 67, 68] is quantified by the large wavelength modes of $g(r/d)$, or equivalently, by the structure factor $S(k)$ at small wave-number k. We calculate $S(k)$ by a direct FFT (fast Fourier transform) of the two-dimensional density. Before we apply the FFT we map the particles onto a $M \times M$ lattice, where M is the closest power of 2 that gives a lattice box size of about one diameter.

The structure factors obtained by ED are presented in Fig. 7(a) and those obtained by DSMC in Fig. 7(b). Different symbols correspond to different times. We observe an increase of $S(k)$ for short wavenumbers $k < 25$, until the structure factor ceases to change for $t \geq 20\,\mathrm{s}$. The structure factor agrees reasonably well for both simulation methods, and for large enough times it does not

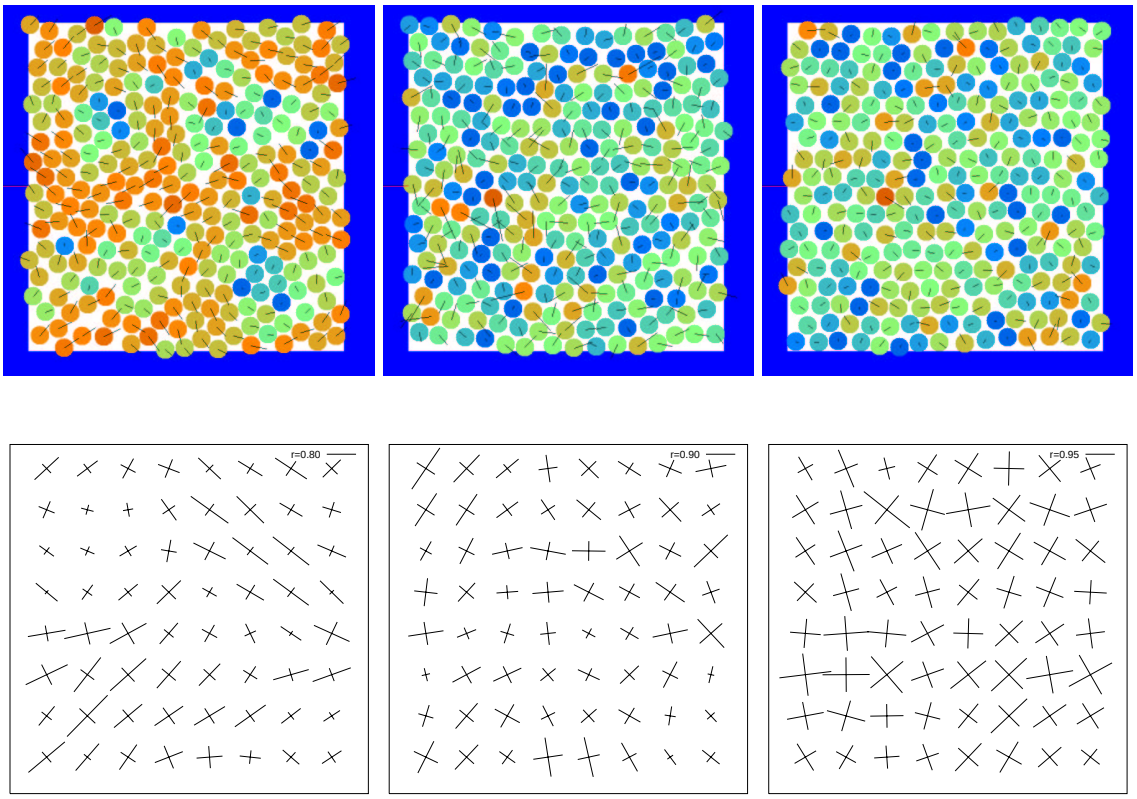

Figure 5: Snapshots from ED simulations in 2D with $N = 240$, $\varrho = 0.7495$ and different $r = 0.80$ (left), $r = 0.90$ (middle), $r = 0.95$ (right) after $t = 1\,\mathrm{s}$. The lines give the velocity vector scaled by 1, 3, and 7 in the left, middle and right panel, respectively. In the panels below the stress is plotted in the principal axis representation following Eq. (9). The average is taken in the time interval $0.5\,\mathrm{s} \leq t \leq 1.0\,\mathrm{s}$ over all collisions in each cell. The maximum eigenvalues $\sigma_{\max}$, measured in the left, middle, and right panel are 0.894, 0.568, and 1.56, respectively. They are measured in arbitrary units and the figures are scaled so that $\sigma_{\max}$ has the same length.

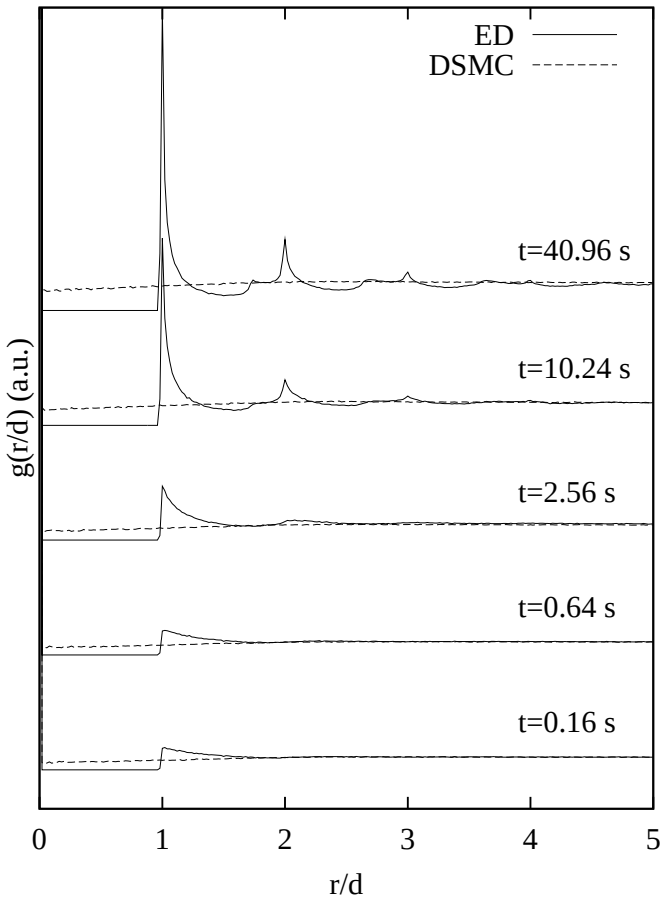

Figure 6: Correlation function $g(r/d)$ as obtained from the ED (solid line) and DSMC (dashed line) simulations of Fig. 2. The different curves are shifted vertically in order to avoid overlap.

change further. This proves that the DSMC simulation is capable to reproduce the more realistic, but computationally more expensive, ED results that account for the excluded volume by construction. Even without short-range correlations, the information about large wavelengths is well reproduced by DSMC simulations.

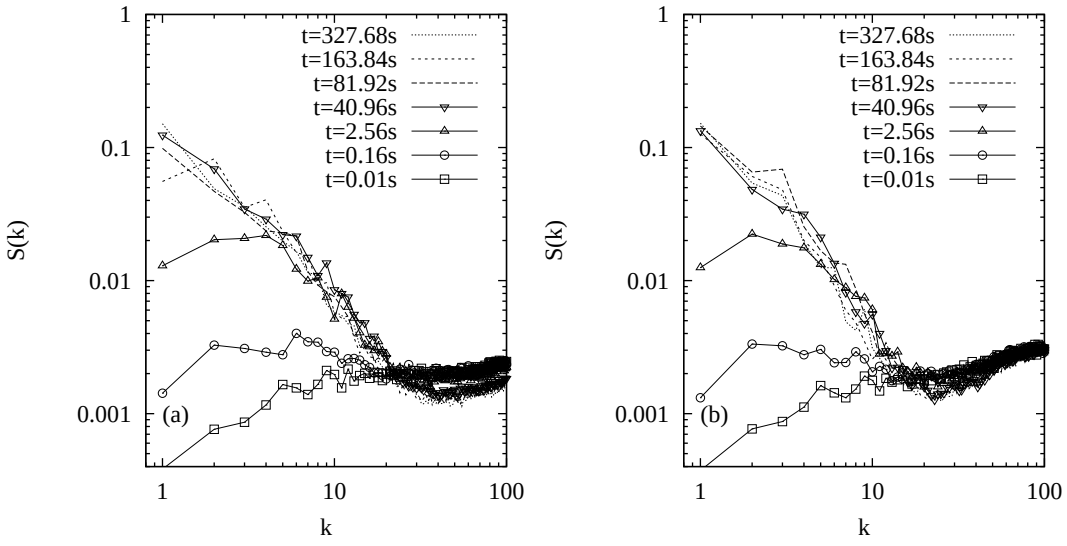

Figure 7: (a) Structure factor obtained from the ED simulations of Fig. 2 as function of the wavenumber $k = l/\lambda$, with wavelength λ and system size l. (b) Structure factor obtained from the corresponding DSMC simulation.

4 The clustering instability

The essential difference between a granular and a classical gas is dissipation. The resulting clustering instability was examined in 1D [35–38, 71–73] and in 2D [10, 42, 68, 74–78]. Cluster growth could be described theoretically only in the case of irreversible aggregation [76, 79], the more general case of reversible aggregation is still an open issue.

Detailed examination of the inelastic collapse by McNamara and Young [68] led to the picture of different 'phases'. In a periodic system without external forcing exists a critical dissipation — connected to volume fraction and restitution coefficient — above which clustering occurs and below which the system stays in molecular chaos. In the transient regime the system behavior seems to depend on the system size and shearing modes are frequently observed.

4.1 Parameter studies

In the following we examine periodic systems of length $L = l/d$ in 2D, with the particle diameter d, using the TCED simulation method as described in subsection 2.2. The volume fraction is $\varrho = N\pi(d/2l)^2 = (\pi/4)N/L^2$ and the particles are initially arranged on a square lattice, homogeneously distributed in the system. First the system is equilibrated with $r = 1$, then the dissipation is switched to the desired value and the simulation starts at $t = 0\,\mathrm{s}$. Here we use a rather small system with $N = 784$, $L = 50$, and $\varrho \approx 0.25$.

The restitution coefficient and the cut-off time t_c are varied ($0.99 \leq r \leq 0.20$ and $10^{-10}\,\mathrm{s} \leq t_c \leq 10^{-3}\,\mathrm{s}$) and the simulation is performed for each parameter set until every particle carried out $C/N = 1000$ collisions. In Fig. 8(a) $K(t)$ is plotted against the mean number of collisions per particle C/N for simulations with $t_c = 10^{-6}\,\mathrm{s}$ and variable r. For large r and small C/N the energy behaves as $K(t) \propto \exp(-C/N)$ as can be derived from Eq. (18) by integration over the product of mean velocity $\overline{v} = \sqrt{K/m}$ and inverse mean free path $\lambda \propto 1/\varrho$. With decreasing r the initial slope is larger because more energy is dissipated per collision. At larger times, energy decays much slower and $K(t)$

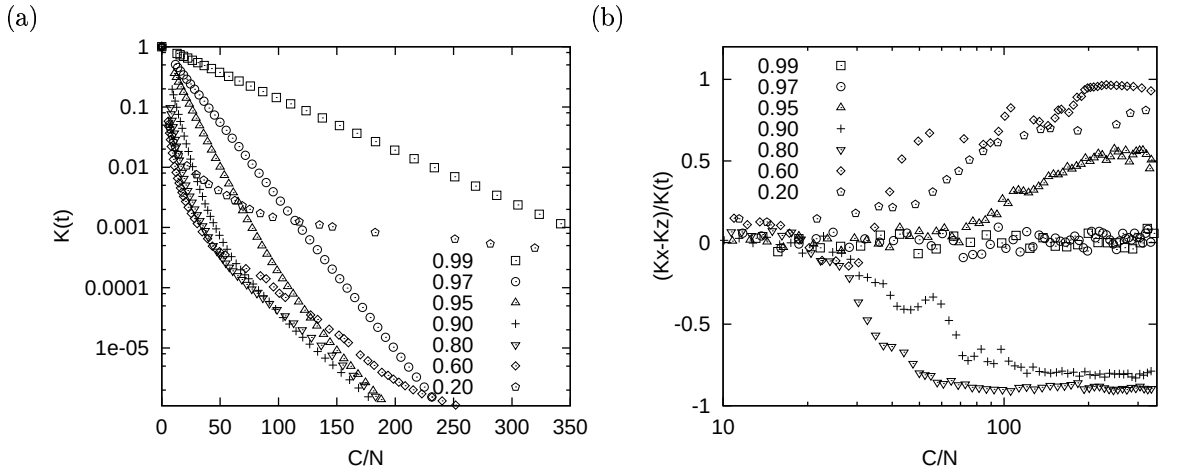

Figure 8: (a) $K(t)$ as function of C/N with $t_c = 10^{-6}$ s and r as given in the insert. (b) $(K_x - K_z)/K(t)$ for the same simulations as in (a).

deviates from the straight line already for $r \leq 0.95$. In Fig. 8(b) $(K_x - K_z)/K(t)$ is plotted against C/N. In a homogeneous system without clustering, the value of $(K_x - K_z)/K(t)$ fluctuates around zero, while values close to unity indicate the 'shearing-mode', i.e. most of the kinetic energy can be found in one direction [80, 81]. The deviations from the homogeneous cooling state begin earlier with decreasing r.

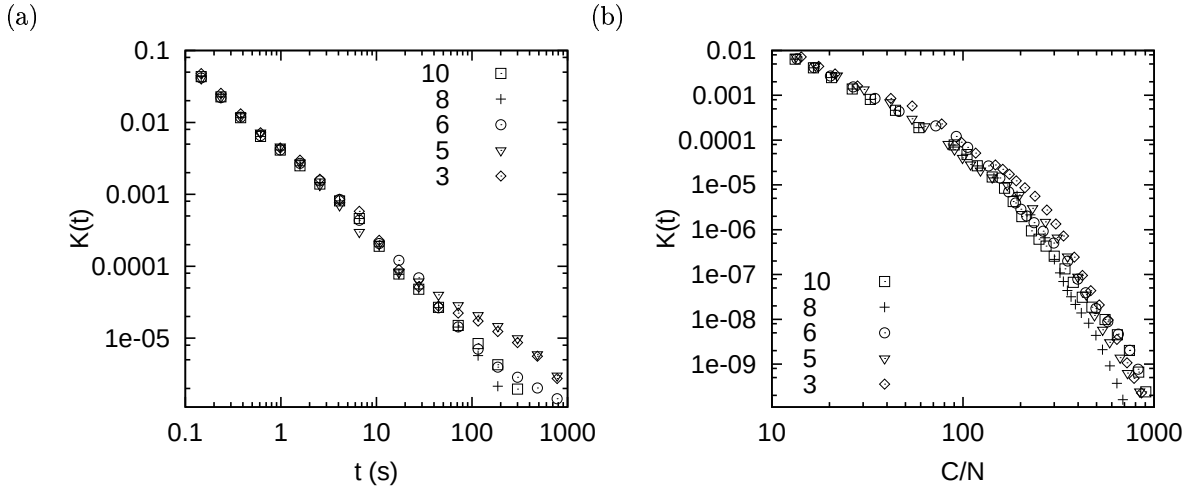

Figure 9: (a) $K(t)$ as function of t with $r = 0.6$ and $-\log_{10} t_c$ as given in the insert. (b) $K(t)$ plotted against C/N for the same simulations as in (a).

For strong dissipation one observes jumps in C/N — meaning that a few particles perform many collisions without affecting the global energy too much. In that case one expects that the time between collisions drops below the threshold t_c and r is set to unity according to Eq. (7). The kinetic energy $K(t)$ is plotted against C/N in Fig. 9(a) for simulations with $r = 0.60$ and different $t_c = 10^{-10}$ s, 10^{-8} s, 10^{-6} s, 10^{-5} s, and 10^{-3} s. For $t < 50$ s the decay of energy is almost independent of t_c. For larger times the simulations with greater t_c loose less energy since more collisions are elastic. From the plot of $K(t)$ against C/N in Fig. 9(b) one observes for $C/N < 100$ a power-law behavior $K(t) \propto (C/N)^{\zeta}$ with $\zeta \approx 2.5$ and for $C/N > 100$ a much faster decay of energy, with $\zeta \approx 7$.

4.2 Cluster growth

In the following we discuss a simulation with $N = 79524$ particles, $L = 500$, $\varrho = 0.25$, and $t_c = 10^{-5}$ s in more detail. In Fig. 10(a) the energy $K(t)$ is plotted against the simulation time. The solid line indicates a slope of -2 as one would get in the homogeneous cooling regime, see Eq. (18). However, the simulation seems to follow, in average, a slope of -1, as indicated by the dashed line. Thus the cooling is much slower when it is non-homogeneous. Fig. 10(b) shows that the fraction of particles that have collisions with a collision frequency larger than $1/t_c$ is only about 0.1 percent of the total number of particles for $t < 50$ s. For larger times, the number of elastic collisions increases, but never above three percent of C/N.

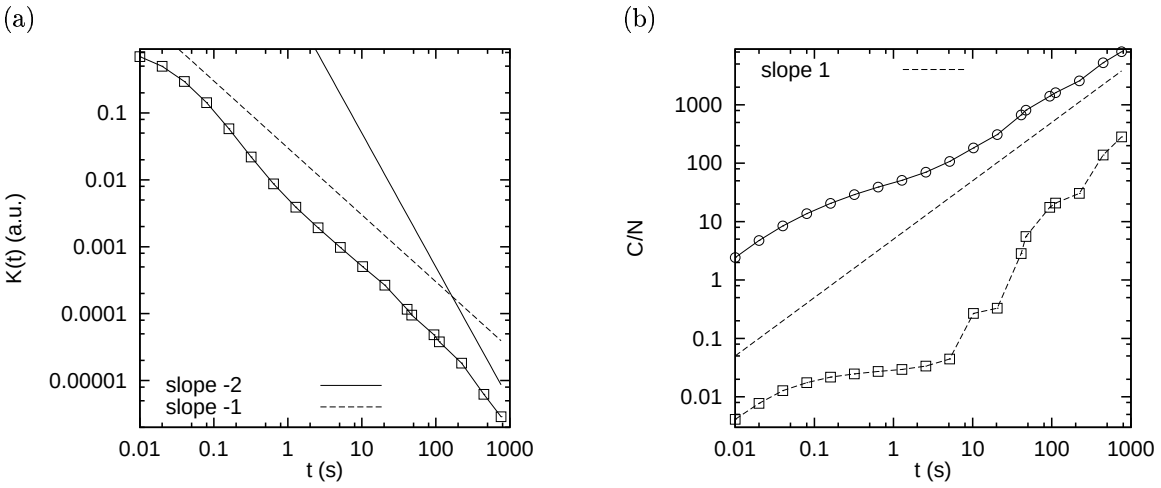

Figure 10: (a) $K(t)$ as function of time t for a simulation with $N = 79524$, $L = 500$, $\varrho = 0.25$, and $t_c = 10^{-5}$ s. (b) C/N as function of t for the simulation in (a). The circles give the mean number of collisions per particle and the squares give the mean number of elastic collisions per particle.

In Fig. 11 snapshots of the simulation in Fig. 10 are displayed. With increasing time t (and C/N) structures build up in the system and grow in size. In the bright regions in the centers of the clusters the collision frequency is largest.

4.3 Probability distribution of the collision frequency

For a more quantitative analysis of the clustering instability, the probability distribution for particle collision frequencies is examined. $P(N_c)$ gives the probability to find a particle that carried out N_c collisions per unit time in the last time interval $\Delta t = t/2$, and it is normalized to unity. In Fig. 12(a) $P(N_c)$ is plotted for the homogeneous cooling during short times. The shape of $P(N_c)$ resembles a Poisson distribution with decreasing mean for $C/N \leq 39$. For $C/N = 8$, i.e. $t = 0.04$ s, the dashed line corresponds to $P_o(\mathcal{C}/\Delta t, 6.5)\,\Delta t$ with the Poisson distribution for the number of collisions $\mathcal{C}$ per particle per time Δt

$$P_o(\mathcal{C}, \chi) = \frac{\exp(-\chi)\chi^{\mathcal{C}}}{\mathcal{C}!} \ , \tag{20}$$

with mean and width $\chi/\Delta t = 6.5/0.02\,\mathrm{s} = 325\,\mathrm{s}^{-1}$. This indicates that the collisions are uncorrelated events at the beginning of the simulation.

At longer times, the probability for a large number of collisions can be well fitted by an exponential

$$P_e(N_c, A) = \frac{1}{A} \exp\left(-\frac{N_c}{A}\right) \ , \tag{21}$$

with the mean collision rate $A = 19\ \mathrm{s}^{-1}$ in Fig. 12(a). As soon as clustering occurs, the form of the probability of the number of collisions changes. In Figs. 12(b) and (c), $P(N_c)$ is displayed at different

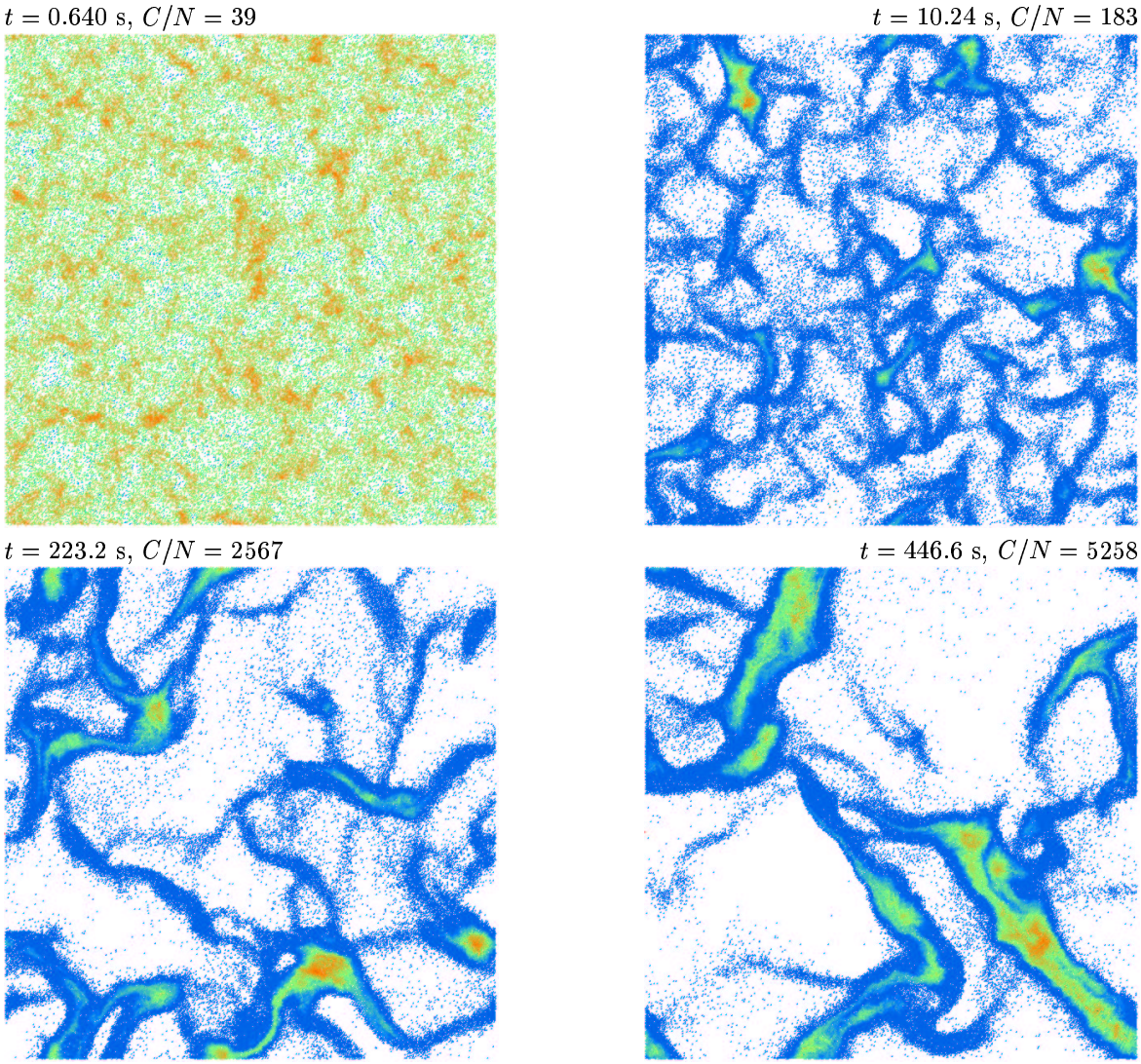

Figure 11: ED simulation with $N = 79524$ particles in a system of size $L = 500$, volume fraction $\varrho = 0.25$, restitution coefficient $r = 0.8$, and critical collision frequency $1/t_c = 10^5$ s^{-1}. The collision frequency is coded in grayscales — dark and light correspond to small and large collision frequencies, respectively.

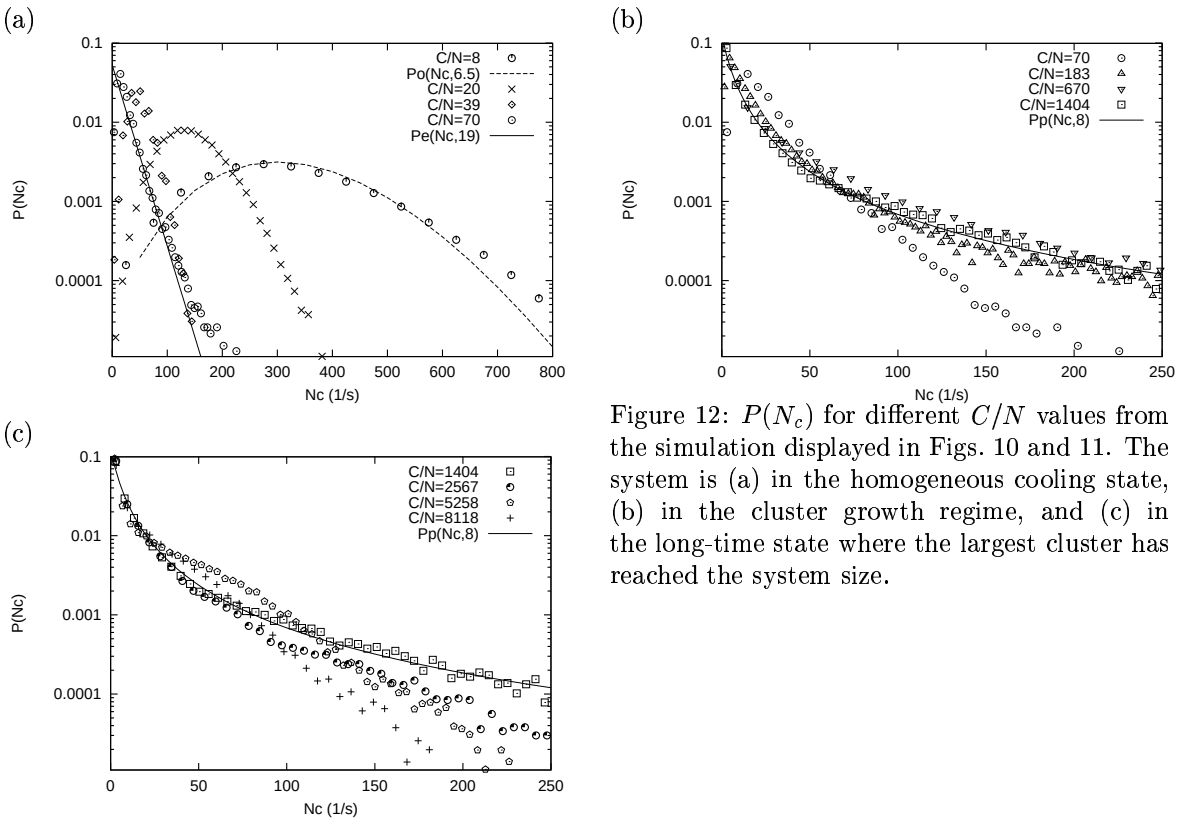

Figure 12: $P(N_c)$ for different C/N values from the simulation displayed in Figs. 10 and 11. The system is (a) in the homogeneous cooling state, (b) in the cluster growth regime, and (c) in the long-time state where the largest cluster has reached the system size.

times, i.e. different C/N. The probability for large (small) collision frequencies increases (decreases), and can now be approximated by a power-law of the form

$$P_p(N_c, B) = \frac{B}{(B + N_c)^2} \ , \tag{22}$$

with the rate $B = 8\ \mathrm{s}^{-1}$. All functions $P(N_c)$ are normalized for arbitrary χ, A or B, but the mean of $P_p(N_c, B)$ diverges. This indicates the inelastic collapse, i.e. the divergence of the global collision frequency. However, in the simulation presented here, the collision frequency is limited since t_c is non-zero.

In summary, we found that for $C/N > 70$ the shape of $P(N_c)$ changes from an exponential decay for large N_c to a power-law behavior. This corresponds to the density instability when clusters evolve and grow with time, i.e. cooperative motion and interaction. Interestingly, the shape of the probability distribution is only weakly varying over one order of magnitude in time, from $C/N \approx 183$ to $C/N \approx 1404$. At these times, particles that carry out many collisions coexist with those which carry out only a few. For even larger times $C/N > 2567$ the function $P(N_c)$ changes shape again, as displayed in Fig. 12(c). The probability for large collision frequencies drops again.

5 Simulating the Flow through Pipes

In this section we present another collective phenomenon in a totally different geometry. Recent observations of approximately V-shaped *microcracks* in vertically vibrated sand-piles [82] led to the problem of gravity driven vertical motion of sandpiles in 2D pipes [7–9, 83]. In this situation the material is accelerated by the gravitational force and confined to the pipe by two side walls. During the fall, cracks develop in the lower part of the pile and ascend progressively inside the bulk in both experiment and simulation [7]. For details on experiments and simulations see Refs. [7, 9].

The reasons for a crack to open have been identified as the fluctuations of either the wall surface [7] and the random particle motion [9]. It was reported that fluctuations lead to a momentum wave in the material. A part of the material is decelerated and the material from above hits this slower plug and causes a new, possibly stronger momentum wave. The increased pressure on the sidewalls may

lead to an even stronger deceleration so that eventually a crack opens below the plug — and becomes visible only that late. Thus, cracks are a rather bad indicator of the dynamical processes occuring inside a granular material, since they need some time to open, before they get visible. In simulations one has access to quantities that allow deeper insight what is going on in the material. The number of collisions per unit time in which a particle participates can be measured and visualized easily.

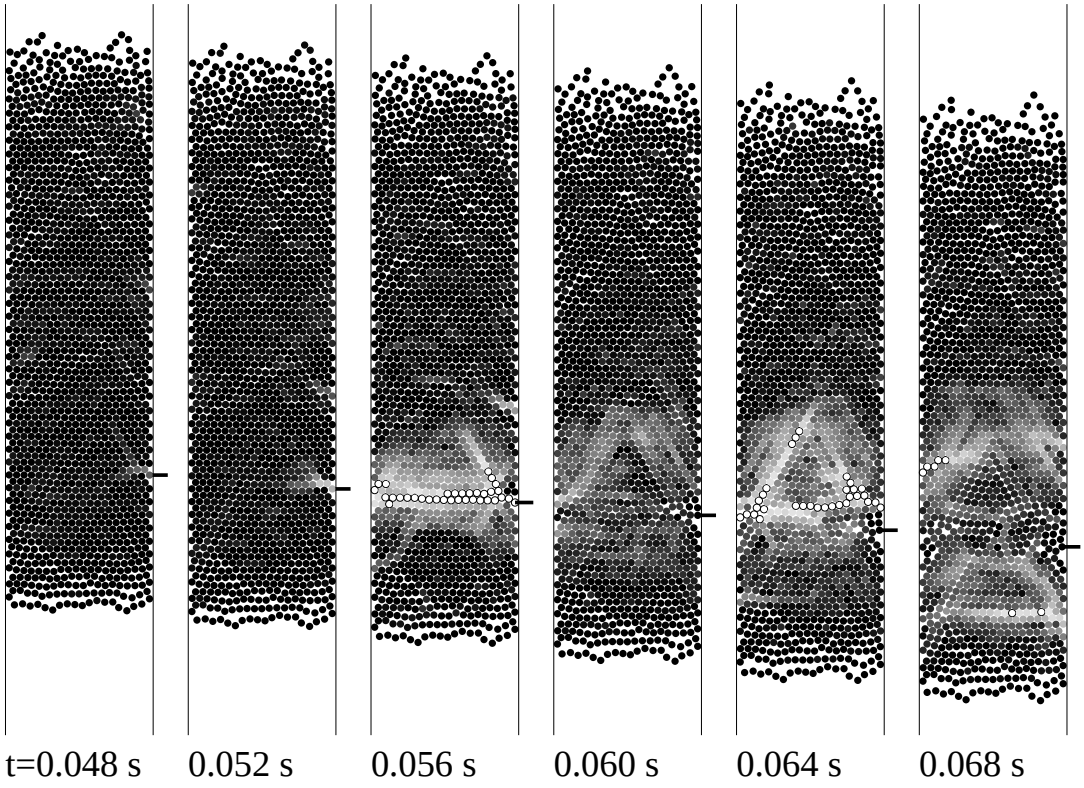

Figure 13: Snapshots from a simulation with $N = 1562$, $L = 20.2$, $\epsilon = \epsilon_w = 0.9$, $\mu = \mu_w = 0.5$, and $\beta_0 = \beta_{0w} = 0.2$. Black particles have a collision frequency of $N_c = 0\,\mathrm{s}^{-1}$, white particles have a frequency larger than $N_c \geq 10^4\,\mathrm{s}^{-1}$, and gray particles interpolate between the two extremes.

The system is a box of width L and initially filled with N particles with diameter d, situated on a triangular lattice with lattice constant $s = 1.01\,d$. Each particle is assigned a random velocity, uniformly distributed in the range $-v_0 \leq v_i(0) \leq v_0$ in both, the horizontal and vertical directions. This rather regular system is now allowed to reach a steady state, i.e. we start the simulation at $t = -t_r$, using $r = r_w = 1$ and $\mu = \mu_w = 0$. A typical average velocity in our simulations is $\overline{v} = \sqrt{< v^2 >} = 0.05\ \mathrm{m\,s}^{-1}$ for $t = 0\,\mathrm{s}$. Due to the rather low kinetic energy, the array of particles is still arranged on a triangular lattice, except for a few layers at the top which are fluidized. In a typical simulation, we use $L = 20.2\,d$ and $N = 1562$, so that the array consists of about 80 layers. At time $t = 0\,\mathrm{s}$ we remove the bottom, switch on dissipation and friction and let the array fall. In Fig. 13 we present data from one special simulation with $N = 1562$, $L = 20.2$, $\epsilon = \epsilon_w = 0.9$, $\mu = \mu_w = 0.5$ and $\beta_0 = \beta_{0w} = 0.2$. Light (dark) particles carried out many (few) collisions in the last interval $\Delta t = 0.001$ s.

The black bar at the right wall marks the particle at which one observes at first a large collision frequency N_c at time $t = 0.048$ s. Already 0.004 s later the neighboring particles react and also carry out more and more collisions. This increase in collision frequency leads to an increase of pressure that, in return, leads to more friction, a slow down of the particles close to the wall, and to even more collisions with the following particles. The gray region indicates an arch like structure that spans the whole width of the system at $t = 0.056$ s. Again 0.004 s later this region of large N_c and large pressure has almost disappeared, and for $t \geq 0.060$ s at the position of the initiating particle (at the black bar) a crack is visible. Even later, new arches above and below the original one appeared.

In Fig. 14 we present again the probability $P(N_c)$ to find a particle in the system that performed a number of N_c collisions per unit time within the last time interval $\Delta t = 0.005$ s. $P(N_c)$ is calculated from the simulation in Fig. 13 at times $t = 0.02$ s, 0.03 s, 0.04 s, and 0.05 s, i.e. before the first arch (or crack) occurs. The probability for the number of collisions can be well fitted by the exponential $P_e(N_c, A)$, see Eq. (21), with the mean collision rate $A = 1$ s^{-1}.

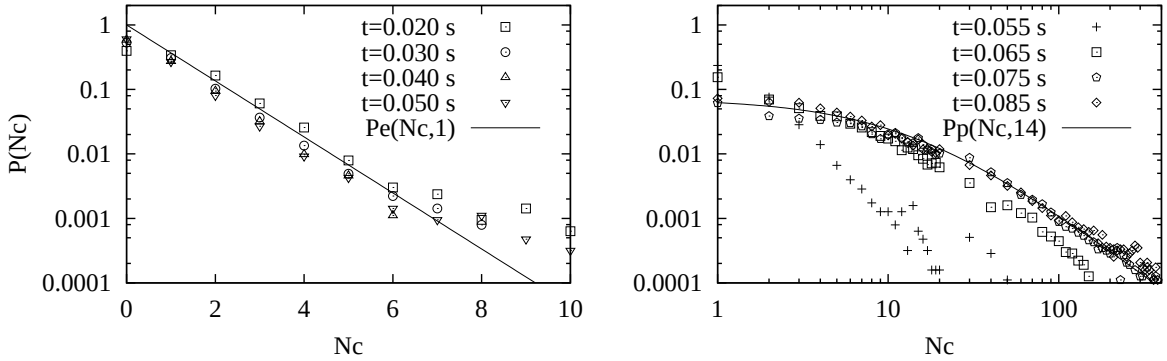

Figure 14: (a) Semi-log plot of the probability distribution $P_e(N_c, A)$ against the number of collisions per unit time from the simulation in Fig. 13. The data correspond to a time before cracks and arching occurs. (b) Log-log plot of $P_p(N_c, B)$ from the same simulation as in (a); here data are presented when cracks and arches exist.

As soon as arches occur, the probability of the number of collisions changes shape. In Fig. 14(b), $P(N_c)$ is displayed at times $t = 0.055$ s, 0.065 s, 0.075 s, and 0.085 s. The probability for large (small) collision frequencies increases (decreases), and can now be approximated by the power-law $P_p(N_c, B)$ with the rate $B = 14$ s^{-1} from Eq. (22). Note that the curves in Fig. 12 and Fig. 14 are similar, the only look different because the horizontal axis is linear in the former case but logarithmic in the latter.

6 Summary and Conclusion

With a rather simple description of a granular material as an ensemble of inelastic spherical particles we have investigated interesting effects like the clustering instability and arching. A freely cooling granulate builds up a density instability and clusters of particles are formed. The structure on small length scales was described with the event driven simulation, but could not be reproduced by the stochastic DSMC method. The large scale structures, i.e. the structure factor of the clusters, however, was nicely reproduced with the stochastic method.

DSMC assumes molecular chaos. Thus we examined different systems and found in 2D a constant probability distribution for the impact parameter, i.e. molecular chaos, when the system is elastic or slightly inelastic. Only for large densities, large systems and strong dissipation, the molecular chaos assumption becomes invalid. In those cases, we observed shearing motion of grains, a phenomenon that can be found also in large, dilute systems after dense clusters have formed. DSMC cannot model dense clusters and also ED has problems to handle dense regions with large collision frequencies. Therefore, we introduced the advanced TCED method that avoids the inelastic collapse, i.e. dissipation is switched off when too much collisions occur per unit time. We found that this variation of the traditional ED method involves only a small percentage of the particles and thus does not afect the system behavior as long as the cut-off time t_c is small enough.

Finally, the statistics of the particle collision frequencies was examined for two totally different boundary conditions. In both cases, freely cooling and pipe flow as well, the probability distribution of the collision frequencies shows two types of behavior. In the homogeneous, random regime the distribution resembles a Poisson distribution (i.e. an exponential for small mean values), indicating that the collisions are uncorrelated events. As soon as cooperative effects like clustering or arching occur, the probability distribution changes from an exponential to a power-law shape. We proposed one functional form that approximated the distribution functions measured from simulations, for both boundary conditions used.

The described cooperative phenomena are e.g. of local nature but leave a fingerprint, i.e. a

power-law, in the global distribution function. An open issue is the theoretical verification and understanding of the shape of the probability distribution function.

Achnowledgements

We thank E. Clément, M. Müller, and S. Weinketz for helpful discussions, and acknowledge the financial support of the Deutsche Forschungsgemeinschaft (SFB 382).

References

[1] D. E. Wolf and P. Grassberger, editors. *Friction, Arching and Contact Dynamics*. World Scientific, Singapore, 1997.

[2] R. P. Behringer and J. T. Jenkins, editors. *Powders & Grains 97*. Balkema, Rotterdam, 1997.

[3] S. Luding. Surface waves and pattern formation in vibrated granular media. In *Powders & Grains 97*, Amsterdam, 1997. Balkema.

[4] H. J. Herrmann, J.-P. Hovi, and S. Luding, editors. *Physics of dry granular media - NATO ASI Series*, Dordrecht, 1998. Kluwer Academic Publishers.

[5] G. W. Baxter, R. P. Behringer, T. Fagert, and G. A. Johnson. Pattern formation in flowing sand. *Phys. Rev. Lett.*, 62(24):2825, 1989.

[6] J. Duran, T. Mazozi, E. Clément, and J. Rajchenbach. Decompaction modes of a two-dimensional "sandpile" under vibration: model and experiments. *Phys. Rev. E*, 50(4):3092–3099, 1994.

[7] J. Duran, T. Mazozi, S. Luding, E. Clément, and J. Rajchenbach. Discontinuous decompaction of a falling sandpile. *Phys. Rev. E*, 53(2):1923, 1996.

[8] S. Luding, J. Duran, T. Mazozi, E. Clément, and J. Rajchenbach. Simulations of granular flow: Cracks in a falling sandpile. In D. E. Wolf, M. Schreckenberg, and A. Bachem, editors, *Traffic and Granular Flow*, Singapore, 1996. World Scientific.

[9] S. Luding, J. Duran, E. Clément, and J. Rajchenbach. Simulations of dense granular flow: Dynamic arches and spin organization. *J. Phys. I France*, 6:823–836, 1996.

[10] I. Goldhirsch and G. Zanetti. Clustering instability in dissipative gases. *Phys. Rev. Lett.*, 70(11):1619–1622, 1993.

[11] F. Melo, P. B. Umbanhowar, and H. L. Swinney. Transition to parametric wave patterns in a vertically oscillated granular layer. *Phys. Rev. Lett.*, 72(1):172–175, 1994.

[12] S. Luding, E. Clément, J. Rajchenbach, and J. Duran. Simulations of pattern formation in vibrated granular media. *Europhys. Lett.*, 36(4):247–252, 1996.

[13] P. B. Umbanhowar, F. Melo, and H. L. Swinney. Localized excitations in a vertically vibrated granular layer. *Nature*, 382:793–796, 1996.

[14] S. Luding. *Die Physik trockener granularer Medien*. Logos Verlag, Berlin, 1998. Habilitation thesis (in german) accepted 1997, ISBN 3-89722-064-4.

[15] S. B. Savage. Gravity flow of cohesionless granular materials in chutes and channels. *J. Fluid Mech.*, 92:53, 1979.

[16] J. T. Jenkins and S. C. Cowin. Theories for flowing granular materials. In S. C. Cowin, editor, *Mechanics Applied to the Transport of Bulk Materials*, New York, 1979. Am. Soc. Mech. Eng.

[17] P. K. Haff. Grain flow as a fluid-mechanical phenomenon. *J. Fluid Mech.*, 134:401–430, 1983.

[18] G. M. Homsy, R. Jackson, and J. R. Grace. Report of a symposium on mechanics of fluidized-beds. *J. Fluid Mech.*, 236:477, 1992.

[19] H. Hwang and K. Hutter. A new kinetic model for rapid granular flow. *Continuum Mech. Thermodyn.*, 7:357–384, 1995.

[20] A. Goldshtein and M. Shapiro. Mechanics of collisional motion of granular materials. Part 1. General hydrodynamic equations. *J. Fluid Mech.*, 282:75–114, 1995.

[21] S. Luding. Collisions & contacts between two particles. In H. J. Herrmann, J.-P. Hovi, and S. Luding, editors, *Physics of dry granular media - NATO ASI Series*, page 285, Dordrecht, 1998. Kluwer Academic Publishers.

[22] J. Javier Brey, M. J. Ruiz-Montero, and D. Cubero. Homogeneous cooling state of a low-density granular flow. *Phys. Rev. E*, 54:3664–3671, 1996.

[23] J.W. Dufty and A. Santos. Practical kinetic model for hard sphere dynamics. *Phys. Rev. Lett.*, 77(7):1270–1273, 1996.

[24] M. P. Allen and D. J. Tildesley. *Computer Simulation of Liquids.* Oxford University Press, Oxford, 1987.

[25] B. D. Lubachevsky. How to simulate billards and similar systems. *J. of Comp. Phys.*, 94(2):255, 1991.

[26] P. A. Cundall and O. D. L. Strack. A discrete numerical model for granular assemblies. *Géotechnique*, 29(1):47–65, 1979.

[27] D. C. Rapaport. *The Art of Molecular Dynamics Simulation.* Cambridge University Press, Cambridge, 1995.

[28] K. L. Johnson. *Contact Mechanics.* Cambridge Univ. Press, Cambridge, 1989.

[29] S. Luding, H. J. Herrmann, and A. Blumen. Scaling behavior of 2-dimensional arrays of beads under external vibrations. *Phys. Rev. E*, 50:3100, 1994.

[30] O. R. Walton and R.L. Braun. Viscosity, granular-temperature, and stress calculations for shearing assemblies of inelastic, frictional disks. *Journal of Rheology*, 30(5):949–980, 1986.

[31] S. F. Foerster, M. Y. Louge, H. Chang, and K. Allia. Measurements of the collision properties of small spheres. *Phys. Fluids*, 6(3):1108–1115, 1994.

[32] L. Labous, A. D. Rosato, and R. Dave. Measurements of collision properties of spheres using high-speed video analysis. preprint, 1997.

[33] S. Luding. Granular materials under vibration: Simulations of rotating spheres. *Phys. Rev. E*, 52(4):4442, 1995.

[34] S. Luding, M. Müller, and S. McNamara. The validity of "molecular chaos" in granular flows. In *Proceedings of the World Congress on Particle Technology*, Brighton, 1998. Institution of Chemical Engineers. to appear.

[35] B. Bernu and R. Mazighi. One-dimensional bounce of inelastically colliding marbles on a wall. *J. Phys. A: Math. Gen.*, 23:5745, 1990.

[36] S. McNamara and W. R. Young. Inelastic collapse and clumping in a one-dimensional granular medium. *Phys. Fluids A*, 4(3):496, 1992.

[37] S. McNamara and W. R. Young. Kinetics of a one-dimensional granular medium in the quasielastic limit. *Phys. Fluids A*, 5(1):34, 1993.

[38] S. Luding, E. Clément, A. Blumen, J. Rajchenbach, and J. Duran. Studies of columns of beads under external vibrations. *Phys. Rev. E*, 49(2):1634, 1994.

[39] Y. Du, H. Li, and L. P. Kadanoff. Breakdown of hydrodynamics in a one-dimensional system of inelastic particles. *Phys. Rev. Lett.*, 74(8):1268–1271, 1995.

[40] G. Giese and A. Zippelius. Collision properties of one-dimensional granular particles with internal degrees of freedom. *Phys. Rev. E*, 54:4828, 1996.

[41] T. Aspelmeier, G. Giese, and A. Zippelius. Cooling dynamics of a dilute gas of inelastic rods. submitted, 1997.

[42] P. Deltour and J.-L. Barrat. Quantitative study of a freely cooling granular medium. *J. Phys. I France*, 7:137–151, 1997.

[43] E. L. Grossman, T. Zhou, and E. Ben-Naim. Towards granular hydrodynamics in two-dimensions. *Phys. Rev. E*, 55:4200, 1997.

[44] M. D. Shattuck, C. Bizon, P. B. Umbanhowar, J. B. Swift, and H. L. Swinney. 2d vertically vibrated granular media: Experiment and simulation. In *Powders & Grains 97*, Rotterdam, 1997. Balkema.

[45] S. Luding, E. Clément, A. Blumen, J. Rajchenbach, and J. Duran. Anomalous energy dissipation in molecular dynamics simulations of grains: The "detachment effect". *Phys. Rev. E*, 50:4113, 1994.

[46] S. Luding, E. Clément, A. Blumen, J. Rajchenbach, and J. Duran. Interaction laws and the detachment effect in granular media. In *Fractal Aspects of Materials*, volume 367, page 495, Pittsburgh, Pennsylvania, 1995. Materials Research Society, Symposium Proceedings.

[47] L. D. Landau and E. M. Lifshitz. *Elasticity Theory*. Pergamon Press, Oxford, 1975.

[48] G. Kuwabara and K. Kono. Restitution coefficient in a collision between two spheres. *Japanese Journal of Applied Physics*, 26(8):1230–1233, 1987.

[49] N. V. Brilliantov, F. Spahn, J. M. Hertzsch, and T. Pöschel. Model for collisions in granular gases. *Phys. Rev. E*, 53(5):5382, 1996.

[50] J. Lee and H. J. Herrmann. Angle of repose and angle of marginal stability: Molecular dynamics of granular particles. *J. Phys. A*, 26:373, 1993.

[51] J. Schäfer, S. Dippel, and D. E. Wolf. Force schemes in simulations of granular materials. *J. Phys. I France*, 6:5–20, 1996.

[52] F. Radjai, J. Schäfer, S. Dippel, and D. Wolf. Collective friction of an array of particles: A crucial test for numerical algorithms. *J. Phys. I France*, 7:1053, 1997.

[53] T. Pöschel and V. Buchholtz. Static friction phenomena in granular materials: Coulomb law vs. particle geometry. *Phys. Rev. Lett.*, 71(24):3963, 1993.

[54] O. R. Walton and R.L. Braun. Simulation of rotary-drum and repose tests for frictional spheres and rigid sphere clusters. In *DOE/NSF Workshop on Flow of Particulates and Fluids*, pages 1–17, 1993.

[55] O. R. Walton. Effects of interparticle friction and particle shape on dynamic angles of repose via particle-dynamics simulation. In *Workshop: Mechanics and Statistical Physics of Particulate Materials*, 1994.

[56] T. Pöschel and V. Buchholtz. Molecular dynamics of arbitrarily shaped granular particles. *J. Phys. I France*, 5(11):1431–1455, 1995.

[57] V. Buchholtz and T. Pöschel. Numerical investigations of the evolution of sandpiles. *Physica A*, 202:390, 1994.

[58] V. Buchholtz, T. Pöschel, and H.-J. Tillemans. Simulation of rotating drum experiments using non-circular particles. *Physica A*, 216:199, 1995.

[59] G. A. Kohring, S. Melin, H. Puhl, H. J. Tillemans, and W. Vermöhlen. Computer simulations of critical, non-stationary granular flow through a hopper. *Comput. Methods in Appl. Mechanics and Eng.*, 124:2273, 1995.

[60] H.-G. Matuttis and S. Luding. The effect of particle shape and friction on the stresses in heaps of granular media. In D. E. Wolf and P. Grassberger, editors, *Friction, Arching and Contact Dynamics*, Singapore, 1997. World Scientific.

[61] L. Brendel and S. Dippel. Lasting contacts in molecular dynamics simulations. In H. J. Herrmann, J.-P. Hovi, and S. Luding, editors, *Physics of Dry Granular Media*, page 313, Dordrecht, 1998. Kluwer Academic Publishers.

[62] G. A. Bird. *Molecular Dynamics and the Direct Simulation of Gas Flow.* Oxford Science Publications, Oxford, 1994.

[63] T. Tanaka, S. Yonemura, K. Kiriba Yashi, and Y. Tsuji. Cluster formation and particle-induced instability in gas-solid flows predicted by the dsmc method. *JSME Int. Journal B*, 39(2):239–245, 1996.

[64] M. Müller, S. Luding, and H. J. Herrmann. Simulations of vibrated granular media in 2d and 3d. In D. E. Wolf and P. Grassberger, editors, *Friction, Arching and Contact Dynamics*, Singapore, 1997. World Scientific.

[65] D. Bideau and A. Hansen, editors. *Some geometrical properties of two-dimensional hard disk packings*, pages 1–34. Disorder and granular media. North-Holland, Amsterdam, 1993.

[66] Francis J. Alexander, Alejandro L. Garcia, and Berni J. Alder. A consistent boltmann algorithm. *Phys. Rev. Lett.*, 74:5212–5215, 1995.

[67] I. Goldhirsch, M.-L. Tan, and G. Zanetti. A molecular dynamical study of granular fluids I: The unforced granular gas in two dimensions. *Journal of Scientific Computing*, 8:1–40, 1993.

[68] S. McNamara and W. R. Young. Dynamics of a freely evolving, two-dimensional granular medium. *Phys. Rev. E*, 53(5):5089–5100, 1996.

[69] J. T. Jenkins and M. W. Richman. Kinetic theory for plane flows of a dense gas of identical, rough, inelastic, circular disks. *Phys. of Fluids*, 28:3485–3494, 1985.

[70] S. Luding, M. Huthmann, S. McNamara, and A. Zippelius. Homogeneous cooling of rough dissipative particles: Theory and simulations. submitted April, 1998.

[71] E. L. Grossman and B. Roman. Density variations in a one-dimensional granular system. *Phys. Fluids*, 8:3218, 1996.

[72] A. Kudrolli and J. P. Gollub. Studies of cluster formation due to collisions in granular material. In *Powders & Grains 97*, page 535, Rotterdam, 1997. Balkema.

[73] A. Kudrolli, M. Wolpert, and J.P. Gollub. Cluster formation due to collisions in granular material. *Phys. Rev. Lett.*, 78(7):1383–1386, 1997.

[74] M. Sibuya, T. Kawai, and K. Shida. Equipartition of particles forming clusters by inelastic collisions. *Physica A*, 167:676, 1990.

[75] S. McNamara and W. R. Young. Inelastic collapse in two dimensions. *Phys. Rev. E*, 50(1):R28–R31, 1994.

[76] E. Trizac and J. P. Hansen. Dynamic scaling behavior of ballistic coalescence. *Phys. Rev. Lett.*, 74(21):4114–4117, 1995.

[77] F. Spahn, U. Schwarz, and J. Kurths. Clustering of granular assemblies with temperature dependent restitution and under keplerian differential rotation. *Phys. Rev. Lett.*, 78:1596–1599, 1997.

[78] J. A. G. Orza, R. Brito, T. P. C. van Noije, and M. H. Ernst. Patterns and long range correlations in idealized granular flows. preprint, 1997.

[79] E. Trizac and J. P. Hansen. Dynamics and growth of particles undergoing ballistic coalescence. *J. Stat. Phys.*, 82:1345–1370, 1996.

[80] S. McNamara. Two dimensional granular medium driven by a vibrating wall. preprint, 1996.

[81] I. Goldhirsch and M.-L. Tan. The single-particle distribution function for rapid granular shear flows of smooth inelastic disks. *Phys. Fluids*, 8(7):1752–1763, 1996.

[82] J. Duran, T. Mazozi, E. Clément, and J. Rajchenbach. Size segregation in a two-dimensional sandpile: convection and arching effects. *Phys. Rev. E*, 50(6):5138–5141, 1994.

[83] S. Luding, J. Duran, E. Clément, and J. Rajchenbach. Computer simulations and experiments of dry granular media: Polydisperse disks in a vertical pipe. In *Proc. of the 5th Chemical Engineering World Congress*, San Diego, 1996. AIChE.